Journal of Sustainable Development Indicators

http://www.sdewes.org/jsdi

Year 2026, Volume 2, Issue 1, 2030672

Original Research Article

Harmonic and Reactive Power Compensation by Multilevel Inverters of Grid-connected Photovoltaic System

***A. Lamreoua*[*1], *M. Elouariach*[1]**

[1]Laboratory of Electrical Engineering and Maintenance (LEEM), Higher School of Technology, University of Mohammed I, Oujda, Morocco

e-mail: mostafa14600@gmail.com, a.lamreoua@mail.com

Cite as: Lamreoua, A., Elouariach, M., Harmonic and Reactive Power Compensation by Multilevel Inverters of Grid-Connected Photovoltaic System, J. sustain. dev. indic., 2(1), 2030672, 2026, DOI: https://doi.org/10.13044/j.sdi.d3.0672

ABSTRACT

In this article, we improved the control of the three phase multilevel inverter for a photovoltaic system connected to the grid, in order to minimize the total harmonic distortion of current. This topology being considered as a new converter topology applied to photovoltaic systems and has the advantage of very high-energy efficiency, but has the disadvantage linked to harmonics injected into the grid, which causes switching of states if the number of levels increases, which increases the rate of harmonic distortion. In this paper, an improved control based on sinusoidal control (SPWM) and space vector control (SVPWM) was proposed to improve the control of multilevel inverters. The simulation is based on MATLAB SIMULINK platform is presented for different multilevel inverter topologies with fewer switches and with different control methods and sinusoidal pulse. A detailed comparison of various Sinusoidal Pulse Width Modulation (SPWM) and vector control schemes (SVPWM) is presented in this article with reference to Total Harmonic Distortion (THD<5%) in the output voltage and current of the grid. This control strategy eliminates current harmonics and improves the quality of energy supplied to the grid by the photovoltaic system, and It can be seen that among all the control methods, the THD is minimum at the output of different multilevel inverter topologies.

KEYWORDS

Multilevel inverter, Photovoltaic system, Three-phase inverter, Sinusoidal control, Harmonics distortion, Grid, Total Harmonic Distortion (THD).

INTRODUCTION

In recent years, the growing demand for electricity relative to the population and the inevitable future depletion of conventional sources necessitate the search for alternative sources, such as renewable energy photovoltaic systems [1]. This research has developed considerably and offers enormous potential, particularly for the conversion of electrical energy sources, of which photovoltaic is very profitable and maintenance-free, so the energy storage system is not necessary [2]. Power quality issues are a particular problem for these systems, as sources of harmonic distortion can represent a high proportion of the total or nonlinear loads (NLL) in grid-injection systems [3]. This current leakage increases the total harmonic distortion (THD) of the current, system losses, and poses personnel safety risks [4]. These

* Corresponding author

systems can be considered nonlinear, meaning they are highly complex and it is very difficult to find a model using conventional approaches. Renewable energy sources (RES) are connected to the distribution grid or micro grid (MG) via an interface converter. Thus, the energy transfer process of the photovoltaic system is based on the importance of good price, small size, and high efficiency [5].

The remaining problem is that the intensive use of non-linear loads has led to serious disturbances in the electrical grid, such as harmonics and unbalanced currents. In this context, several solutions have been proposed. Among them, to improve converter efficiency and control, this research can primarily influence one of three aspects: firstly, the converter's structure; in this case, several specific inverter designs have been developed to connect a photovoltaic inverter to the distribution grid [6]. The second aspect is based on improving the technology and selecting its components, more precisely on the choice of semiconductors and filters. Finally, one can influence the modulation applied to the converter (Pulse Width Modulation). Two main modulation families are known: one based on direct current control (current control), and the other on indirect control through the control of a reference average voltage [7].

This article focuses on improving the modulation applied to the converter with different structures. To this end, various types of inverters and control systems can be used to improve the performance of these devices in order to reduce grid pollution and optimize electricity costs.

The harmonic distortion of current (THDi) [8], becomes very high if the current leakage is high, which causes losses of the grid and safety problems for personnel close to the latter [9]. Different types of full-bridge inverters [10], controlled by the sinusoidal control technique (SPWM) are used for the elimination of these current loss problems [11]. Therefore, multilevel converters have been considered a preferred topology for large powers due to their advantages such as high levels, overall efficiency, and high output waveform quality [12]. Against this background, we proposed three-phase and single-phase inverters [13]. These are no longer used to send pure sinusoidal current signals to the grid in phases [14]. To achieve these goals, the choice of these photovoltaic inverters is based on the equivalence between the reactive power supplied and the nominal power consumed by the grid, with the cost of these inverters [15]. It is expressed in terms of power related to the quality of the energy supplied to the grid [16].

Multilevel topologies have emerged to overcome the drawbacks that prevent the use of power converters in higher voltage and current applications [17]. Various multilevel converter topologies have been introduced, each of which has an important advantage that makes them more suitable for particular applications [18]. While the main multilevel topologies focus on the use of many semiconductor devices and main source DC circuits, later, many efforts have been made to optimize conventional multilevel structures [19], or to design a new optimized structure [20]. The optimization was a compromise between the number of output voltages, the number of active and passive devices, and the DC sources [21].

Generally, the switching techniques of multilevel converters are classified into high and low switching frequency methods [22]. Since the multilevel converter includes a considerable number of semiconductor devices, they can generate notable power losses, particularly in high power applications, if high switching frequency modulation techniques are used [23]. On the other hand, the low frequency modulation technique [24] should be optimized in an adaptable manner depending on the targeted application in order to improve the system efficiency and converter performance [25]. In this article, a study and improvement of the control of multilevel inverters and their modulation techniques is presented. This command allows indirect control of the active and reactive powers injected into the grid. The PI controllers are implemented to adjust the grid currents in the synchronous frame. To generate the reference current and maintain synchronism between the inverter and the grid, a Phase-locked loop technique (PLL) can be used. The main advantage

and objective of this method is to effectively compensate the harmonic current content of the grid current. Multilevel converters provide higher quality waveforms, reducing current and voltage ripple after reducing losses caused by high frequency harmonics. Less expensive and less bulky passive components are used, which is to reduce manufacturing costs, gain in efficiency, reliability and energy quality.

The main objective is to address, in terms of cost, efficiency, power management and power quality, the problems found with classic three phase photovoltaic inverter. After comparing the results of the two systems, we notice that the current THDi of the interlaced inverter is lower than that obtained with the classical inverter. The effectiveness of these techniques proposed in this article is demonstrated by the simulation results using the MATLAB / SIMULINK environment.

THREE PHASE MULTI-LEVEL INVERTER MODELING AND CONTROL METHOD

Description of our research system

The shape of the proposed three-phase photovoltaic inverter is proven in **Figure 1**. It includes a PV generator as energy source, an MPPT block to make certain the tracking of the MPPT, a transistor bridge which include a current converter provided through the PV generator and on the cease a clear out to put off harmonics at excessive frequencies.

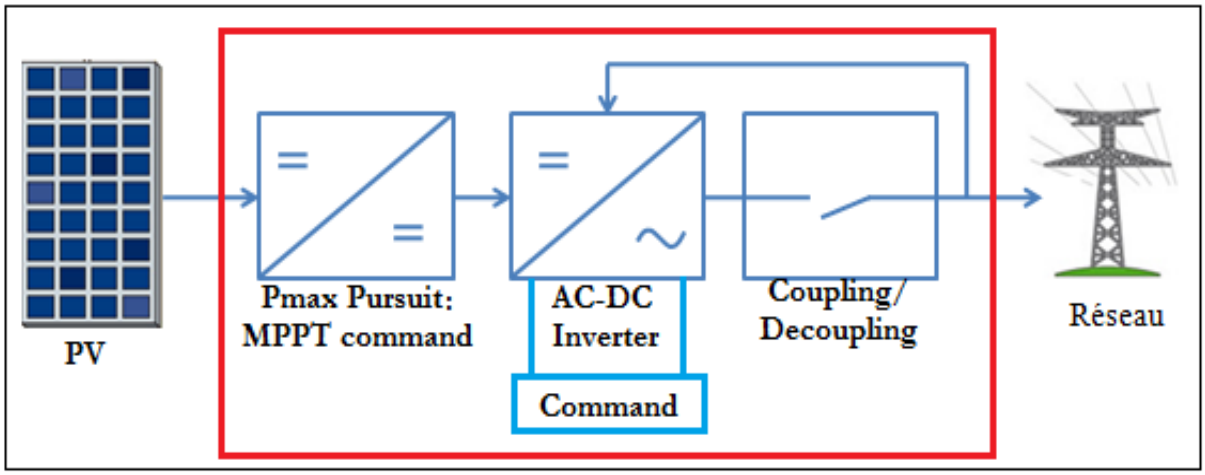

Figure 1. Diagrams of the proposed photovoltaic inverter with the grid

Three-phase multi-level inverter structure

Cascading H-Bridge structure. Cascading H-Bridge seven-level inverter, are obtained by connecting two or more single-phase HBridge inverters, each consisting of four switches, in series, which gives multiple voltage levels at the inverter. Thus, to obtain a seven-level voltage, this inverter consists of 3 H-bridges in series, i.e. 12 switches and a maximum output voltage of 3Vdc. **Figure 2a** shows the CHB seven-level for one phase.

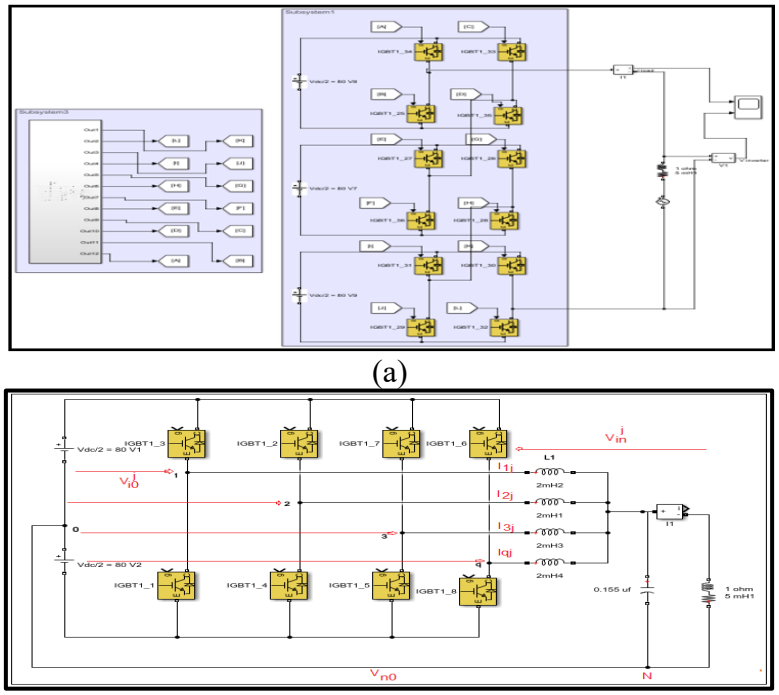

(a)

(b)

Figure 2. (a) Seven-level CHB inverter (one phase);
(b) *PV* Grid-Connected multi-level Interlaced inverter (one phase)

Interlaced inverter structure. **Figure 2b** shows the proposed architecture of the system *PV* connected to the power grid using an interlaced inverter (q =4). Our system consists of a voltage source Vdc, an interlaced inverter, a filter and the grid. In our case study, the q = 4 inductors $L1$ represent the filter inductances on the inverter side. From the **Figure 3**, we will note that the quantities, $Vi0j$ is the voltage vector of cells, $Vinj$ is the voltage vector on the inverter side, $Vj2$ is the voltage vector of the grid, is the vector of the current flowing through the cells of switching of the inverter. q is the number of cells, ijc is the current through the capacitor; $ij1$ and $ij2$ are the output currents on the inverter and grid. The subscript j denotes the number of the phase (j = 1, 2, 3) while i denotes the row of interlaced cells of a phase j (i = 1, 2...q). The inverter is controlled by open loop and closed-loop pulse width modulation (MLI). The diagram of the control command of the inverter is shown in **Figure 3**. The control of the three arms is obtained by comparing a modulating sine wave ($Vj*$; j = 1, 2, 3) of frequency f = 50Hz with q high frequency triangular carrier waves (fsw = 20 kHz). The q carriers are offset by Tsw/q (Tsw being the switching period) and the three-reference sinusoidal voltages $Vj*$ are phase-shifted by $2\pi/3$. The two switches of the same switching cell are complementary $Ki = \overline{Ki'}$ (i = 1, 2, 3...). In this part, we add a balancing loop to the previous command. This control contains two current regulation loops: an external loop for controlling the output current and a loop internal for cell current balancing (**Figure 4**).

Seven-level packed U-Cell inverter structure. The three-hase seven-level MPUC inverter is shown in **Figure 3**. The PUC type multilevel inverter delivers high range of power quality using a small number of active and passive components. This topology comprises a set of arms with two switches and a capacitor. If we have a converter of n arms, the latter will be composed of $2n$ switches and $n-1$ with $2n-1$ levels. Thus, our seven-level converter composed of six switches and two capacitors per phase, on the other hand that of a cascade multi-level inverter consists of 12 switches per phase.

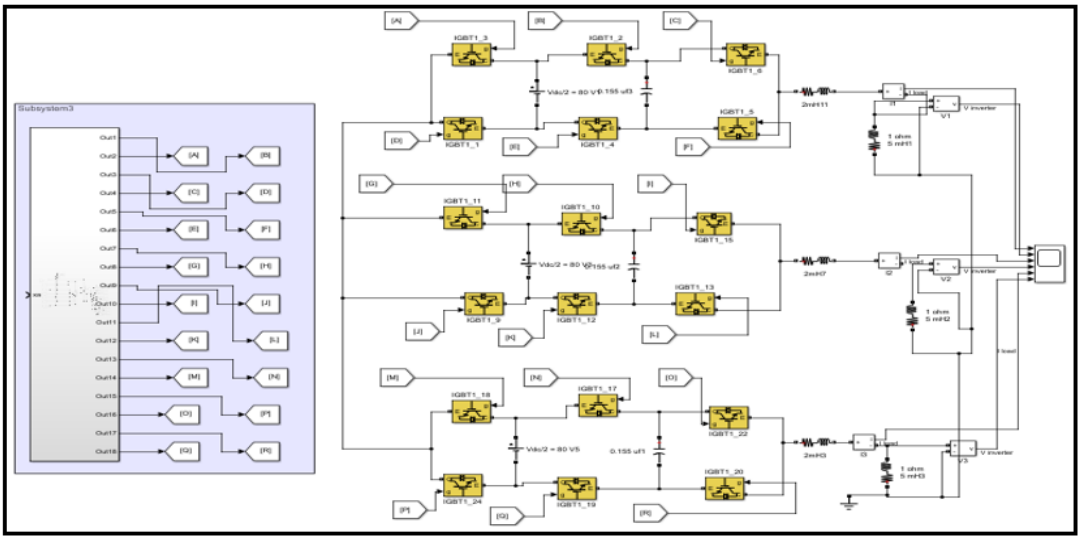

Figure 3. Three phase seven-level packed U-Cell Inverter

It can be noticed that the PUC inverter are only two redundant switching states for the zero-voltage vector and the remaining six states give a unique voltage level at the output. Depending on the voltage and current polarities, the cell capacitors are charged, discharged or bypassed. The PUC-cell inverter has the most minimum number of components compared to the various other structures of multilevel converters.

Control method

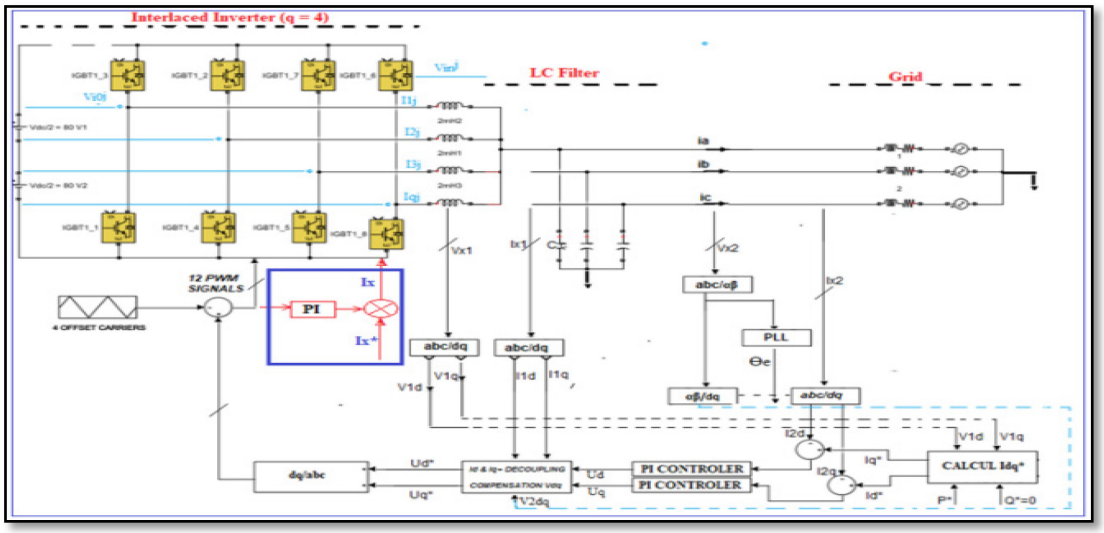

Figure 4. Block illustration of the proposed control system

Mathematical model

The reference currents in the *dq* axis, *I*d* and *I*q*, can be obtained from the following relationships:

$$\begin{bmatrix} u_d \\ u_q \\ u_0 \end{bmatrix} = [L] \begin{bmatrix} u_A \\ u_B \\ u_C \end{bmatrix} \text{ and } \begin{bmatrix} i_d \\ i_q \\ i_0 \end{bmatrix} = [L] \begin{bmatrix} i_A \\ i_B \\ i_C \end{bmatrix} \quad (1)$$

with

$$(I*q=0) \text{ and } [L]=\sqrt{\frac{2}{3}}\begin{bmatrix}\sin\alpha & \sin(\alpha-\frac{2\pi}{3}) & \sin(\alpha+\frac{2\pi}{3})\\ \cos\alpha & \cos(\alpha-\frac{2\pi}{3}) & \sin(\alpha+\frac{2\pi}{3})\\ \frac{1}{\sqrt{2}} & \frac{1}{\sqrt{2}} & \frac{1}{\sqrt{2}}\end{bmatrix} \tag{2}$$

$$\begin{aligned} P=V_{\mathrm{d}}I_{\mathrm{d}}+V_{\mathrm{q}}I_{\mathrm{q}} &\overset{V_{\mathrm{q}}=0}{\Longrightarrow} I^{*}d=\frac{P^{*}}{V_{\mathrm{d}}} \\ Q=V_{\mathrm{d}}I_{\mathrm{q}}-V_{\mathrm{q}}I_{\mathrm{d}} &\overset{V_{\mathrm{q}}=0}{\Longrightarrow} I^{*}{}_{\mathrm{q}}=\frac{Q^{*}}{V_{\mathrm{d}}} \end{aligned} \quad \begin{cases} \frac{d}{dt}V^{2}{}_{\mathrm{DC}}=\frac{2}{C}(P_{\mathrm{in}}-P_{\mathrm{out}}) \\ I_{\mathrm{d}}^{*}=\frac{1}{V_{\mathrm{d}}}(k_{\mathrm{p}}(P_{\mathrm{in}}-P_{\mathrm{out}})+K_{\mathrm{I}}\int(P_{\mathrm{in}}-P_{\mathrm{out}})dt \end{cases} \tag{3}$$

$$\begin{aligned} V_{\mathrm{d}}^{*} &= k_{\mathrm{p}}(I^{*}{}_{\mathrm{d}}-I_{\mathrm{q}})+K_{\mathrm{I}}\int \begin{matrix}((I^{*}{}_{\mathrm{d}}-I_{\mathrm{q}})dt \\ -\omega L_{\mathrm{f}}I_{\mathrm{d}}+V_{\mathrm{d}}\end{matrix} \\ V_{\mathrm{q}}^{*} &= k_{\mathrm{p}}(I^{*}{}_{\mathrm{q}}-I_{\mathrm{q}})+K_{\mathrm{I}}\int \begin{matrix}\left((I^{*}{}_{\mathrm{q}}-I_{\mathrm{q}}\right)dt \\ -\omega L_{\mathrm{f}}I_{\mathrm{q}}+V_{\mathrm{d}}\end{matrix} \end{aligned} \tag{4}$$

Current harmonic control and compensation unit

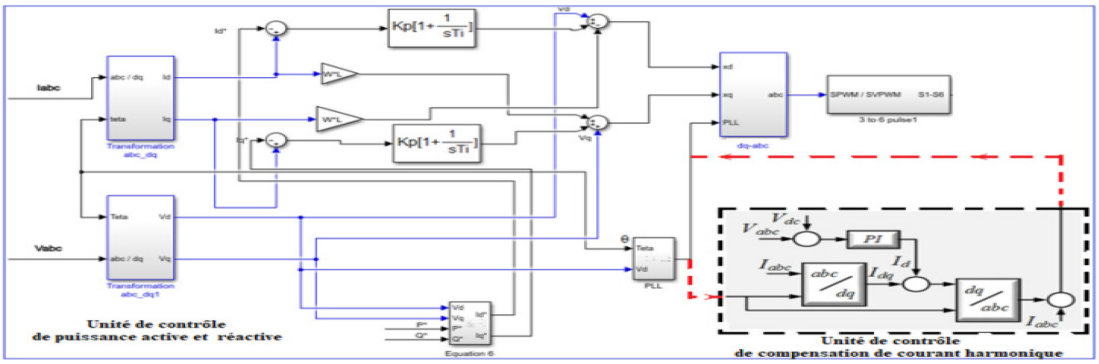

Figure 5. Current harmonic control and compensation unit

Regarding the current harmonic compensation control unit, the input parameters are given by the following equation:

$$\begin{aligned} i_{\mathrm{d}} &= \bar{i_{\mathrm{d}}}+\tilde{i_{\mathrm{d}}} \\ i_{\mathrm{q}} &= \bar{i_{\mathrm{q}}}+\tilde{i_{\mathrm{q}}} \end{aligned} \tag{5}$$

with

$$\begin{aligned} \bar{i_{\mathrm{d}}} &= \frac{1}{2\pi}\int_{0}^{2\pi} i_{\mathrm{d}}d\omega t \\ \bar{i_{\mathrm{q}}} &= \frac{1}{2\pi}\int_{0}^{2\pi} i_{\mathrm{q}}d\omega t \end{aligned} \tag{6}$$

and

$$\begin{aligned} i_{\mathrm{d}} &= \sqrt{\frac{2}{3}}\left[i_{\mathrm{A}}sin\omega t+i_{\mathrm{B}}\sin\left(\omega t-\frac{2\pi}{3}\right)+i_{\mathrm{C}}\sin\left(\omega t+\frac{2\pi}{3}\right)\right] \\ i_{\mathrm{q}} &= \sqrt{\frac{2}{3}}\left[i_{\mathrm{A}}cos\omega t+i_{\mathrm{B}}\cos\left(\omega t-\frac{2\pi}{3}\right)+i_{\mathrm{C}}\cos\left(\omega t+\frac{2\pi}{3}\right)\right] \\ a_{A(i)} &= \sqrt{\frac{2}{3}}\bar{i_{\mathrm{d}}}\,(t) et b_{\mathrm{A}(i)}=\sqrt{\frac{2}{3}}\bar{i_{\mathrm{q}}}\,(t) \end{aligned} \tag{7}$$

Distorted currents :

$$i_s = \begin{bmatrix} i_A \\ i_B \\ i_C \end{bmatrix} = \begin{bmatrix} a_{A(i)} sin\omega t + b_{A(i)} cos\omega t \\ a_{B(i)} sin\left(\omega t - \frac{2\pi}{3}\right) + b_{B(i)} cos\left(\omega t - \frac{2\pi}{3}\right) \\ a_{C(i)} sin\left(\omega t + \frac{2\pi}{3}\right) + b_{C(i)} cos\left(\omega t + \frac{2\pi}{3}\right) \end{bmatrix} \quad (8)$$

Compensating currents:

$$i_{MCP} = i - i_S \quad (9)$$

$$\begin{matrix} u_d \sqrt{\frac{2}{3}\left[u_A \sin wt + u_B \sin (wt - \frac{2\pi}{3}) + u_C \sin (wt + \frac{2\pi}{3})\right]} \\ u_q \sqrt{\frac{2}{3}\left[u_A \cos wt + u_B \cos (wt - \frac{2\pi}{3}) + u_C \cos (wt + \frac{2\pi}{3})\right]} \\ u_0 = \frac{1}{3}(v_A + v_B + v_V) \end{matrix} \quad (10)$$

with

$$\begin{bmatrix} u_d \\ u_q \\ u_0 \end{bmatrix} = [L] \begin{bmatrix} u_A \\ u_B \\ u_C \end{bmatrix} \quad (11)$$

The control variables then become continuous values; therefore, filtering and control can be easily implemented. This method is only applicable to three-phase systems. Since the harmonic current compensation controller processes direct current quantities, its control unit is completely stable. The extracted reference signal is then used to trigger the grid output controller, which will allow the inverter to introduce the desired compensation current into the system.

The PQ current control unit (**Figure 5**). In this part, we directly control the output current into the load, being identical to the sum of the currents of the cells. The current loop generates the reference voltages $Ud*$ and $Uq*$ which are transformed in reverse Park to obtain three sinusoidal voltages in the reference abc.

The transfer function of our system is given by the matrix equation in coordinate's *dq*:

$$G_{PI}^{(dq)}(s) = \begin{bmatrix} K_p + \frac{K_i}{s} & 0 \\ 0 & K_p + \frac{K_i}{s} \end{bmatrix} \quad (12)$$

PR Regulator. The Proportional Resonant Regulator for the current is given by the following expression:

$$GPR(s) = KP + KI\frac{s}{S^2 + \omega 0^2} \quad (13)$$

wherever *KP* and *KI* succinctly represent the proportional gain and the integral gain.

Instantaneous reactive power (IRPT). Instantaneous reactive power theory (IRPT) based control of filter, is designed to work with balanced load currents and balanced as well as undistorted supply voltages. The IRP theory, initially proposed by H. Akagi to regulate active filters [5], relies on a set of instantaneous powers fixed in the time domain. This *p-q* approach is valid for operation under all conditions namely transient and steady-state operation. This theory makes use of some famous transformation models like Clarke's Transformation. Here the voltage and current waveforms are sensed and then made to transform from a-b-c coordinates to $\alpha - \beta - 0$ co-ordinates also known as the Clarke transformation (Figure 6). After this transformation, based on a certain set of equations calculate active and reactive power and then eliminate the power components having harmonics in it by passing through a certain suitable low pass filter of suitable frequency. This can be overcome by individually pre-processing the supply voltages and load currents through the symmetrical sinusoidal integrator for the extraction of the respective positive sequence fundamental components, which can be further processed by the IRPT for the reference current generation.

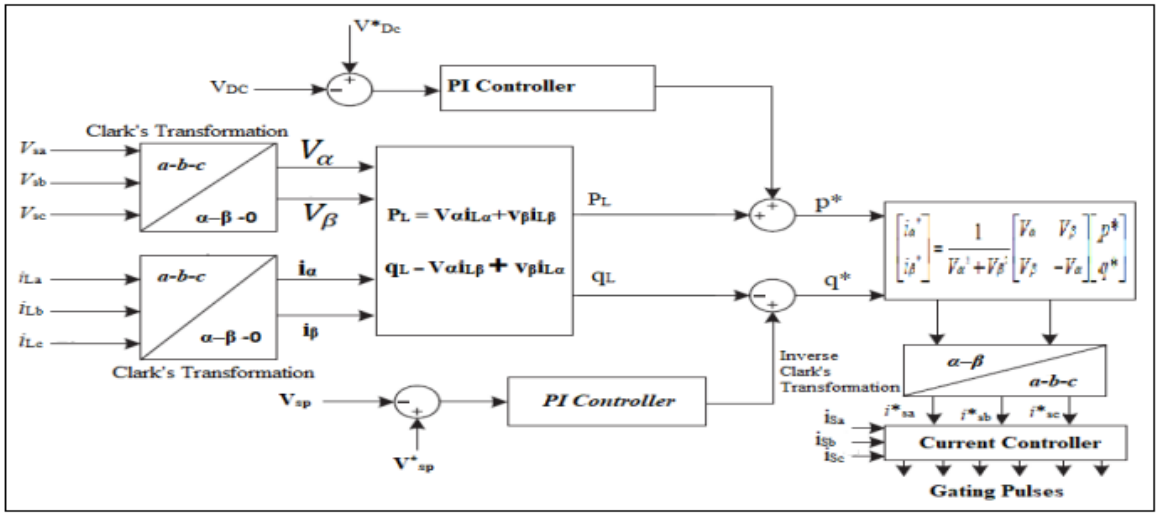

Figure 6. Block diagram of IRP based control algorithm

Transport Delay Based PLL structure. The principle of PLL is to use a PI controller to reduce the phase difference between the line phase angle and the voltage output phase angle to zero (Figure 7).

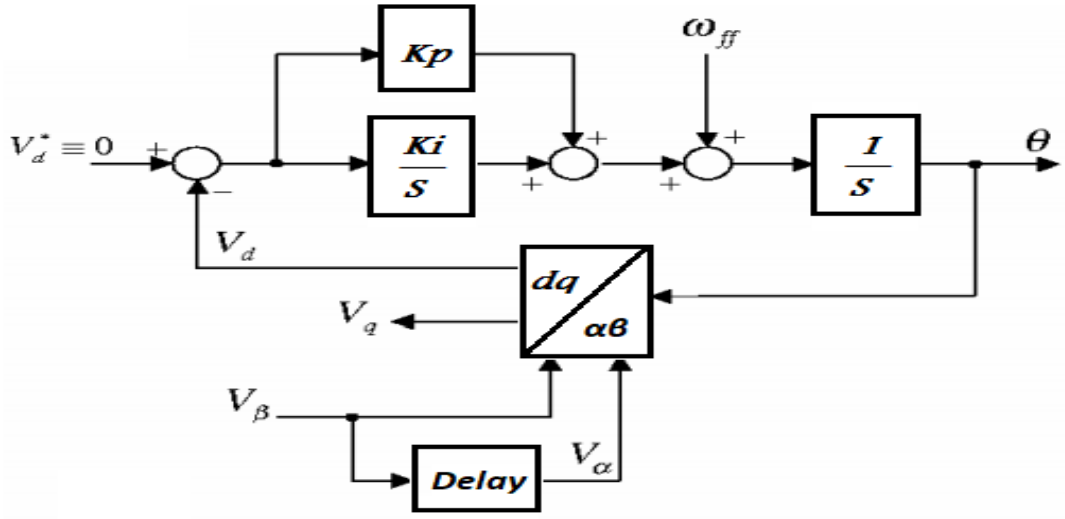

Figure 7. Phase locked loop algorithm

Table 1. Simulation parameters

PV Power	500W
V_d	80V
I_{min}	1A
f_g	50Hz
f_{pwm}	10KHz

SIMULATION RESULTS

After recalling the operating principle of the SPWM and SVPWM command, we will model it under the environment of the MATLAB / SIMULINK software.

Cascading H-Bridge Seven-Level inverter

Sinusoidal Pulse with modulation control (SPWM).

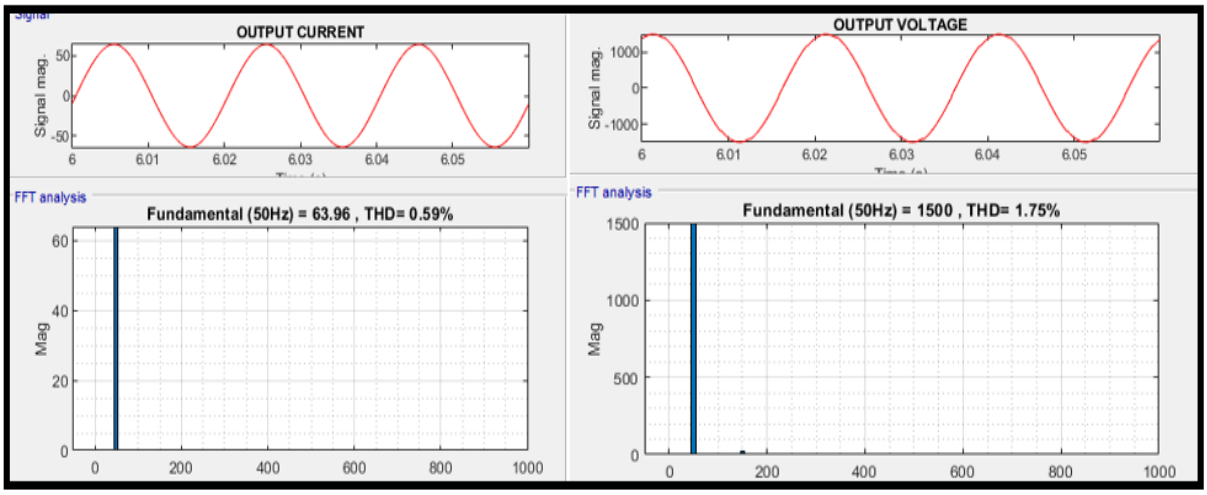

Figure 8. FFT spectrum current and voltage by the SPWM control

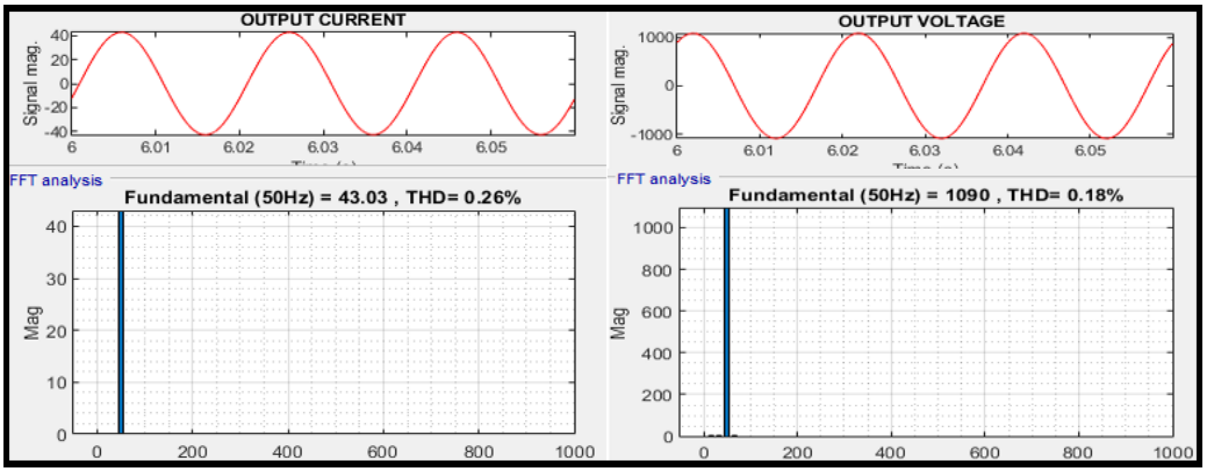

Figure 9. FFT spectrum current and voltage by the SVPWM control

Space vector pulse with modulation control (SVPWM). By applying the same control strategy presented previously, the PWM method is used to generate voltage signals at the output of the inverter. This control method is based on the indirect control of active and reactive currents injected into the grid.

With the SPWM control strategy and from the FFT analysis shown in **Figure 8**, it was possible to see that the total THD of this topology is better and equal to THDi=0.59% and THDv=1.75% for the current and the voltage respectively. With this SPWM control strategy, the THD of the seven levels topology is less than that of the value obtained by an open-loop control, and all the harmonics of high frequencies, disappeared after application of the sinusoidal command, therefore the SPWM control strategy allows us to obtain a purely sinusoidal signal in the grid.

In the second **Figure 9**, the total harmonic distortion observed for the space vector control is THDi=0.26% and THDv=0.18%. The all harmonics are eliminated, using the SVPWM control, providing a reduction in harmonics present at the output of the multi-level inverter.

The benefits of this control were confirmed by the reduced harmonic distortion, as well as the quality of the current and voltage signal at the output of this inverter into the grid.

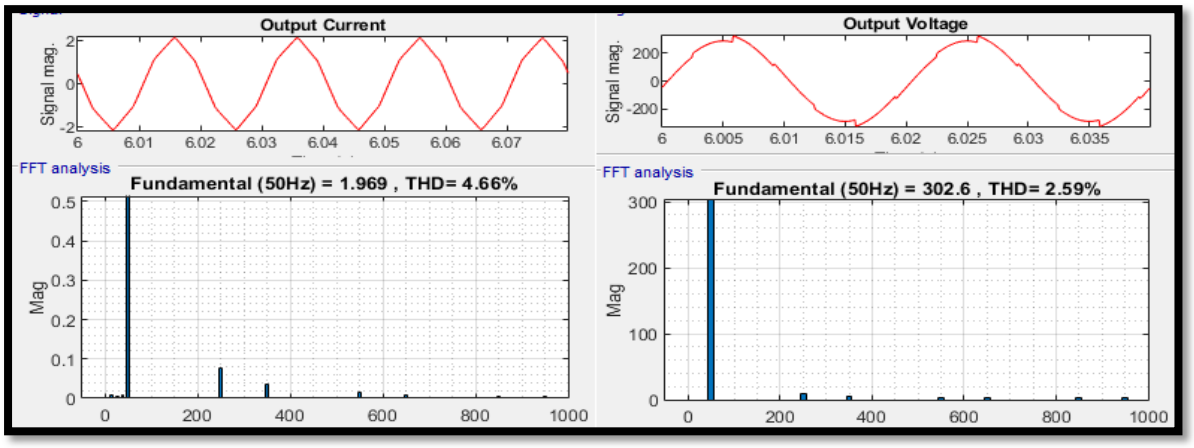

Figure 10. Grid current and voltage FFT spectrums before filtering

Seven-level three-phase inverter (interlaced inverter q = 4)

For the seven-level interleaved inverter, each phase of the inverter is composed of q=4 arms. The control of the three arms is obtained by comparing a modulating sine wave with q triangular carrier waves. In this part, we add a balancing loop to the previous command. This control contains two current regulation loops: an external loop for controlling the output current and a loop internal for cell current balancing.

Before compensation, the current and voltage spectrum obtained in **Figure 10**, the one-shaped output signals are not purely sinusoidal because of the harmonics of currents and voltage. After compensation, the waveforms of the current and voltage in **Figure 11a** and **Figure 11b**, are almost sinusoidal and identical. We can notice the difference between FFT spectrums before and after filtering, such as, after filtering is perfectly sinusoidal while that before filtering is not. The Toral Harmonic Distortion of current and voltage are respectively THDi = 0.28% and THDv = 0.30% for the 50 first harmonics, unlike the indicators of TDH obtained by the system before filtering (4.66% and 2.59%), the indicators TDH of the system using an interlace inverter after filtering are much better. This shows that the TDH indicators of the system using an interlaced inverter are much better than those obtained with the conventional inverter. Therefore, by comparing the results from the spectral analysis, it could be seen that the total THD of the multi-level three-phase interlaced inverter topology is lower than in the two-level three-phase photovoltaic inverter typologies. Thus, we were able to ob-serve a clear improvement in the transient regime and the waveforms in the case of the interlaced inverter system compared to the classic system.

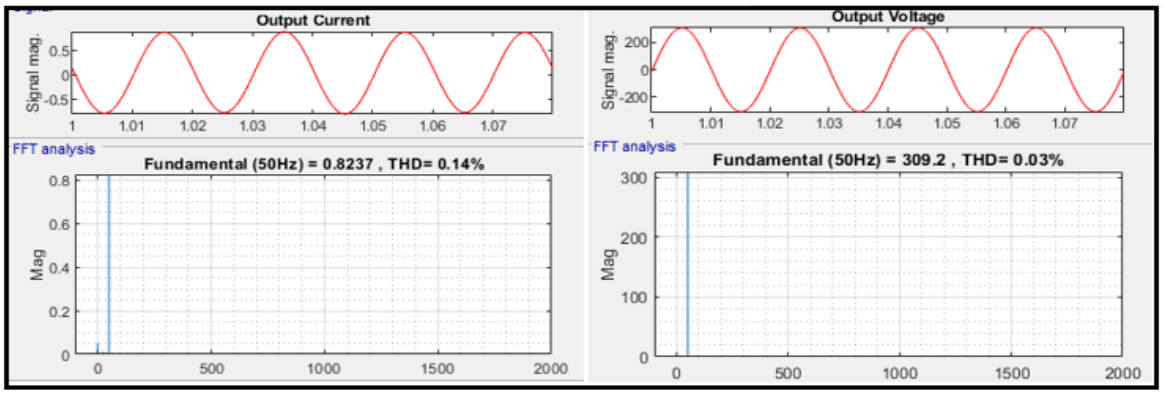

(a)

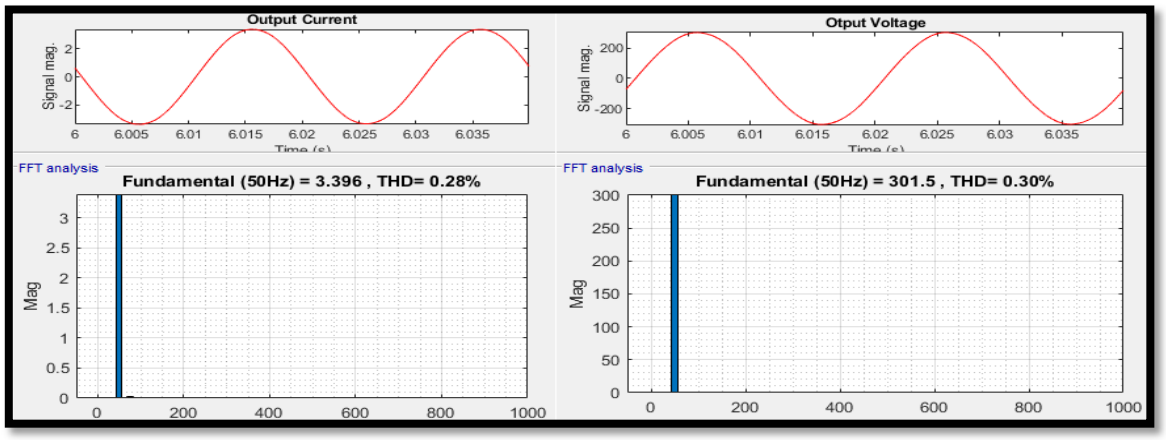

(b)

Figure 11. Grid current and voltage FFT spectrums after filtering: (a) by the SPWM control; (b) by the SVPWM control

Closed-loop control: PUC seven-level inverter

Sinusoidal Pulse with modulation control.

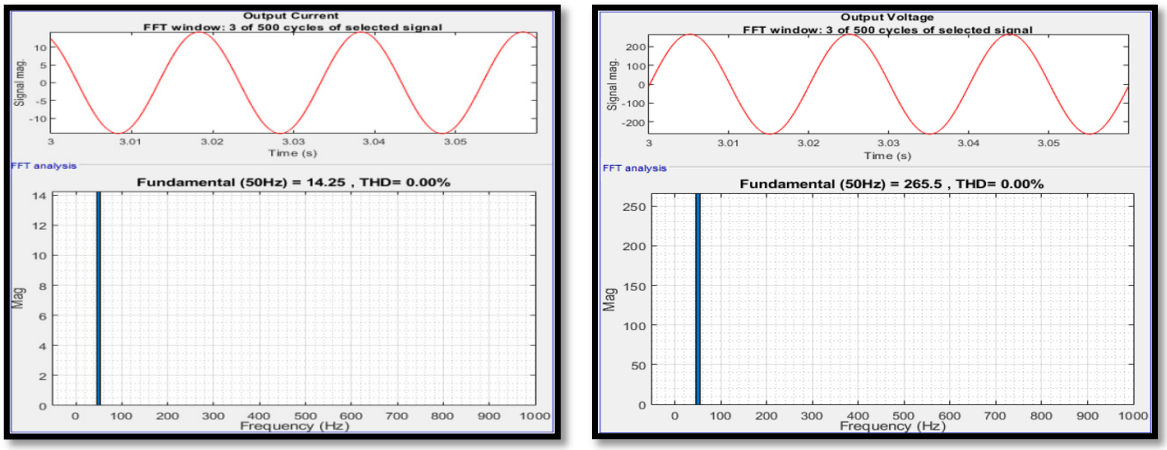

Figure 12. FFT spectrum current and voltage by the SPWM control

Space vector pulse with modulation control (SVPWM).

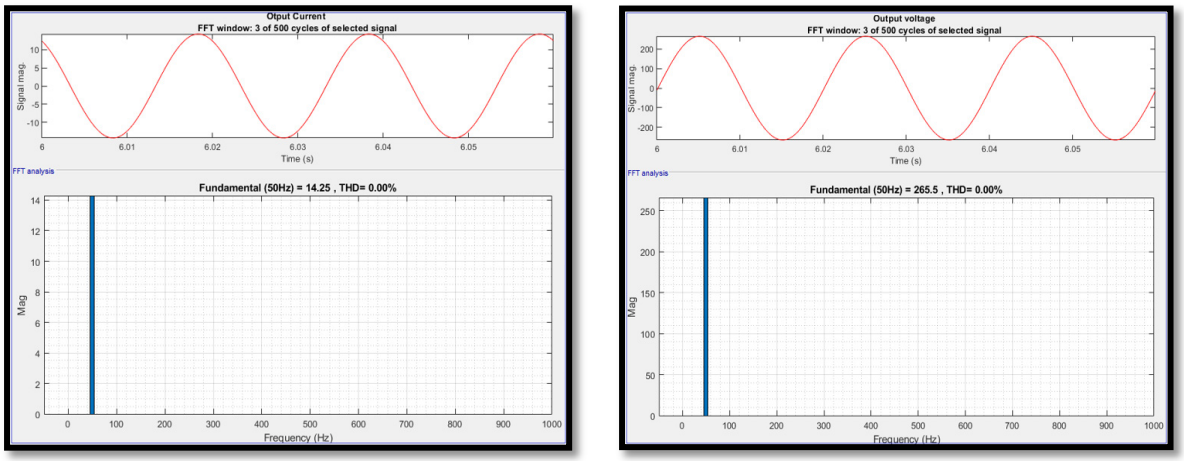

Figure 13. FFT spectrum current and voltage by the SVPWM control

To generate the control reference voltage of the multi-level PUC inverter, this voltage is a sinusoidal waveform based on pulse control with modulation. This reference voltage can be subdivided into six positive and negative intervals after comparison with six triangular signals. Our control method allows indirect control of the active and reactive current delivered in the grid.

An SPWM control simulation of a three-phase seven-level PUC inverter is evaluated for nonlinear overload and the above spectrum is shown the **Figure 12**. The results obtained in closed loop make it possible to produce a purely sinusoidal current and voltage, is illustrated in the **Figure 12** with a THD of 0% for the current and the voltage successively. The load voltages are equal to the reference value, and in phase with the current, with a zero THD (<<<5%).

After application of Vector Pulse Width Modulation (SVPWM), the results obtained by this method are identical to Sinusoidal Control (SPWM), with one difference that, Spatial Vector PWM is a digital modulation method that has previously been used to generate levels of voltage $2N+1$. However, not suitable for high power applications, due to the complexity of vector calculations and associated times. It requires two reference voltages for the upper and lower arms. The waveforms and the THD spectrum for the SVPWM control strategy are shown in **Figure 13**. The current and voltage waveform are purely sinusoidal after applying the SVPWM command. The THD of current and voltage at seven levels is measured at 0.0% respectively. From the simulation results with two control strategies, it is concluded that with the multi-level PUC inverter, the harmonic distortion is less after applying SPWM and SVPWM control. In addition to this, it also has a reduced number of components, which has made it possible to completely improve the conduction losses and the current losses injected into the grid, and finally to have the highest output voltage.

Table 2. Comparison of THD for different controls of the three-phase Seven-Level inverter

Structure	Control strategy	THDi	THDv
Three-Phase seven level interlaced inverter	Closed-loop : SPWM Control	0.28%	0.30%
	Closed-loop : SVPWM Control	0.14%	0.03%
Three-Phase Seven-level CHB Inverter	Closed-loop : SPWM Control	0.59%	1.75%
	Closed-loop : SVPWM Control	0.26%	0.18%
Three-Phase Seven-level PUC Inverter	Open-loop seven-level inverter Control	16.48%	16.48%
	Closed-loop : SPWM Control	0.0%	0.0%
	Closed-loop : SVPWM Control	0.0%	0.0%

From the simulation results with two-control strategies **Table 2**, it is concluded that with the multi-level PUC inverter has less harmonic distortion after applied of SPWM and SVPWM control the grid have been completely improved, and finally has the highest output voltage compared to the interleaved and CHB topology. In addition to this, it also has a reduced number of components, so lower conduction losses and the losses of current injected into the grid, and finally to have the highest output voltage.

EXPERIMENTL RESUTS

In this section, we present an experimental study on a test bench within the laboratory (GEM). The objective of this study is to validate the proposed control principle to improve the quality of the current injected by the three-phase inverter into the grid.

Test bench (LPGEM Laboratory)

In the first part of this section, we present the various pieces of equipment that make up our test bench (three-phase load, voltage inverter, DSP board, etc.), illustrating the technical specifications for each piece of equipment. The second part of this chapter will be devoted to the results obtained from the experimental tests.

a) b) c)

Figure 14. a) Three-phase voltage inverter; b) CLP1104DSP;
c) electronic galvanic isolation board

Current and voltage at the load terminals after connection of a three-phase inverter

In this section, we present the results of SPWM and SVPWM control of the output current and voltage, as well as the current and voltage harmonic distortion, for connecting a three-phase inverter to the grid, both with and without compensation. We also present the DC bus voltage of the inverter used to inject the current. The experimental results are obtained from the waveforms of the voltages and currents injected by the three-phase inverter into the grid.

Figure 15 shows the current and voltage harmonic distortion rates for the three-phase inverter controlled by SPWM and SVPWM without compensation. We observe that the current and voltage harmonic distortion rates exceed the limit set by the standards (5%).

The **Figure 16** shows the current and voltage harmonic distortion rates for the three-phase inverter controlled by SPWM and SVPWM with compensation. We observe that the current and voltage harmonic distortion rates remain within acceptable limits (<5%).

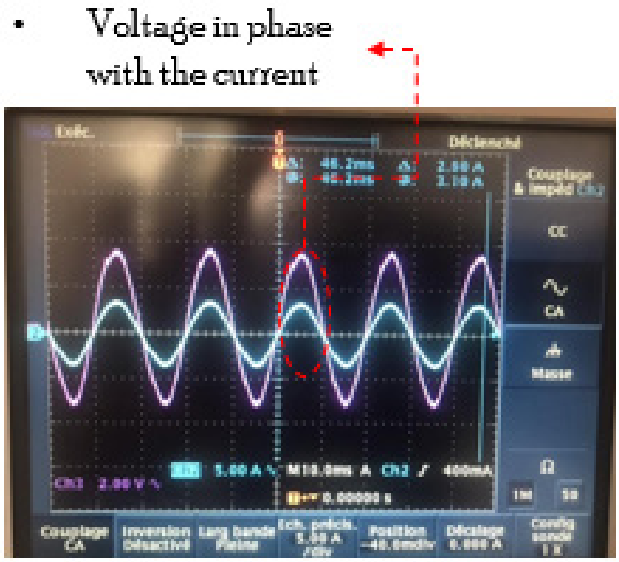

Figure 15. C/V without compensation

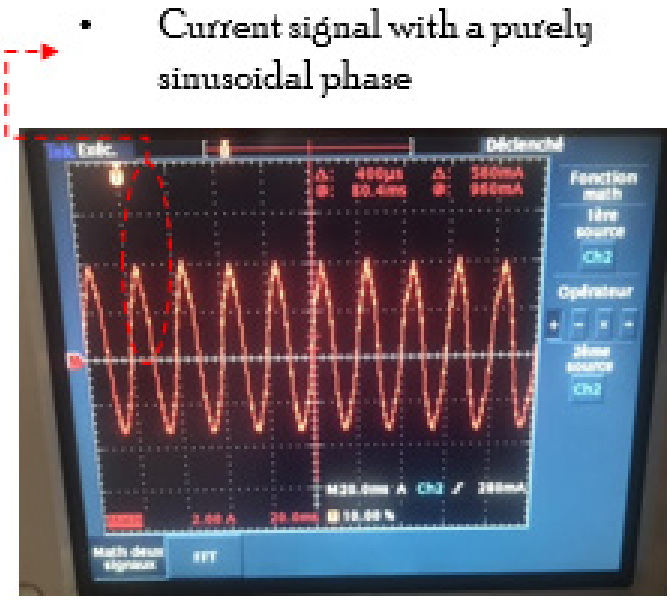

Figure 16. C/V with compensation

The tests performed show that the experimental results converge with those obtained in simulation. Based on these results, we found that the current injection technique based on sinusoidal and vector control provides better performance in harmonic rate compensation within the standards, regardless of changes in load power, which allowed us to achieve the objectives of this regulation.

CONCLUSION

This article is a contribution towards the improvement the control of the three-phase Multi-level photovoltaic inverter, with a new control strategy, by the sinusoidal (SPWM) and space vector (SVPWM) control for a nonlinear load. The comparison of the results of two controls applied to the three-phase photovoltaic inverter at seven levels shows an effective reduction of the THD (<<5%) by the vector control (SVPWM) compared to that of the sinusoidal control (SPWM), with better quality of the current and the voltage injected into the grid by the two control strategies. And our findings suggest that the PUC topology offers

several advantages compared to the interleaved and CHB topology, such as the low THD, the reduced number of components, and the highest output voltage which makes it possible to obtain better performance and a low manufacturing cost. The proposed control scheme presents a simple control structure with satisfactory operating performances that are comparable with those reported with control structures for two level topologies. We result that this control method respond, in terms of cost and energy efficiency, to the problems encountered with the photovoltaic inverter, and effectively compensates the harmonics current injected in the grid. After validation of the experimental results for a two-level three-phase system, the implementation of these simulation results for multi-level three-phase inverters in a complete system is the subject of the next step which allowed us to verify the reliability of these results and achieve the objectives of this regulation.

REFERENCES

1. Shamshuddin, M. A., Kennel, R. M. and Verdugo, D., Nomenclature overview and beat frequency in the family of AC/AC modular multilevel cascade converters (MMCC), IEEE Access, Vol. 13, pp 42064–42082, 2025, https://doi.org/10.1109/ACCESS.2025.3546880.
2. Kihal, A., Talbi, B., Krama, A., Laib, A. and Sahli, A., A multi-functional grid-tied PV system using a split source inverter with energy management and power quality improvement features, IEEE Access, Vol. 13, pp 29789-29800, 2025, https://doi.org/10.1109/ACCESS.2025.3538069.
3. Bengourina, M. R., Direct power control of a grid connected photovoltaic system, associated with an active power filter, Journal of Renewable Energies, Vol. 20, No. 1, pp 99-109, 2017, https://doi.org/10.54966/jreen.v20i1.613.
4. Naderipour, A., Mohd. Zin, A. A., Habibuddin, M. H. B., Miveh, M. R. and Guerrero, J. M., An improved synchronous reference frame current control strategy for a photovoltaic grid-connected inverter under unbalanced and nonlinear load conditions, PLoS ONE, Vol. 12, No. 2, p e0164856, 2017, https://doi.org/10.1371/journal.pone.0164856.
5. Zhang, X., Ma, Z., Gu, B., Fang, L. and Yu, X., On BESS capacity optimization of hybrid coal-fired generator and BESS power station for secondary frequency regulation, IEEE Xplore, Vol. 13, pp 60833–60845, 2025, https://doi.org/10.1109/ACCESS.2025.3557853.
6. Hasan, M. M., Abu-Siada, A. and Islam, Design and implementation of a novel three-phase cascaded half-bridge inverter, IET Power Electronics, Vol. 9, No. 8, pp 1741-1752, 2016, https://doi.org/10.1049/iet-pel.2015.0951.
7. Noman, A. M., Addoweesh, K. E., Alabduljabbar, A. A. and Alolah, A. I., Cascaded H-Bridge MLI and Three-Phase Cascaded VSI Topologies for Grid-Connected PV Systems with Distributed MPPT, International Journal of Photoenergy, p 7642919, 2019, https://doi.org/10.1155/2019/7642919.
8. Wu, Z., Xu, G., Zhu, W. and Sheng, G., A dispersing proportional resonance controller for selective harmonic current compensation in a shunt active power filter, IEEE Transaction on Power Electronics, Vol. 40, No. 1, pp 279–289, 2025, https://doi.org/10.1109/TPEL.2024.3457990.
9. Arévalo-Soler, J., Nahalparvari, M., Groß, D., Prieto-Araujo, E., Norrga, S. and Gomis-Bellmunt, O., Small-signal stability and hardware validation of dual-port grid-forming interconnecting power converters in hybrid AC/DC grids, IEEE Journal of Emerging and Selected Topics in Power Electronics, Vol. 13, No. 1, pp 809–826, 2025, https://doi.org/10.1109/JESTPE.2024.3454992.
10. Hiral, H., Vaidehi, D. and Amit, V. S., Modified symmetrical sinusoidal integrator and instantaneous reactive power theory-based control of shunt active filter, Energy Reports, Vol. 8, Suppl. 13, pp 515–523, 2022, https://doi.org/10.1016/j.egyr.2022.08.151.

11. Lamreoua, A., Benslimane, A., Bouchnaif, J. and El Ouariachi, M., An Improved Sinusoidal (PWM) and Vector (SVPWM) Current Control for a Three-Phase Photovoltaic Inverter Connected to a Non-linear Load, Proceedings of the 2nd International Conference on Electronic Engineering and Renewable Energy Systems, ICEERE 2020., Saidia, Morocco, pp 481-494, April 13-15, 2020, https://doi.org/10.1007/978-981-15-6259-4_51.
12. Azeem, A., Ansari, M. K., Tariq, M., Sarwar, A. and Ashraf, I., Design and Modeling of Solar Photovoltaic System Using Seven-Level Packed U-Cell (PUC) Multilevel Inverter and Zeta Converter for Off-Grid Application in India, Electrica, Vol. 19, No. 2, pp 101-112, 2019, https://doi.org/10.26650/electrica.2019.18053.
13. Odeh, C. I., Kondratenko, D., Lewicki, A., Morawiec, M., Śderko, A. J. and Baran, J., Pulse-Width Modulation Template for Five-Level Switch-Clamped H-Bridge-Based Cascaded Multilevel Inverter, Energies, Vol. 14, p 7726, 2021, https://doi.org/10.3390/en14227726.
14. Lakshmi, T. V. V. S., George, N., Umashankar, S. and Kothari, D. P., Cascaded seven level inverter with reduced number of switches using level shifting PWM technique, International Conference on Power, Energy and Control (ICPEC), Dindigul, India, February 6-8, 2013, https://doi.org/10.1109/ICPEC.2013.6527742.
15. Vu, P., Trang, V. N., Dinh, M. N., Cuong, T. N. and Anh, D. T., Modified space vector modulation technique for three phase three level t-type inverter, International Journal of Renewable Energy Research (IJRER), Vol. 11, No. 3, Sep. 2021, https://ijrer.org/index.php/ijrer/article/view/12058, [Accessed: Feb. 12, 2026].
16. Khalid, H. A., Al-Emadi, N. A., BenBrahim, L., Gastli, A. and Cecati, C., A novel model predictive control with an integrated SOC and floating DC-link voltage balancing for 3-phase 7-level PUC converter-based MV BESS, International Journal of Electrical Power and Energy Systems, Vol. 130, p 106895, 2021, https://doi.org/10.1016/j.ijepes.2021.106895.
17. Uwagboe, U. O. and Saha, A. K., A Comprehensive Review of Multilevel Inverter Topologies and Control Strategies for Grid-Connected Photovoltaic Battery Energy Storage Systems Integrating Active Power Filter, IEEE Access, Vol. 13, pp 169989-170016, 2025, https://doi.org/10.1109/ACCESS.2025.3615104.
18. Lamreoua, A., Benslimane, A. and El Ouariachi, M., An improved sinusoidal (SPWM) and Space Vector (SVPWM) Current Control for Multi-Levels Three-phase Photovoltaic Inverter Connected to a Non-Linear Load, Proceedings of the International Conference on Digital Technologies and Applications (ICDTA 22), Digital Technologies and Applications, Fez, Morocco, Vol. 1, pp 672–683, 2022, https://doi.org/10.1007/978-3-031-01942-5_67.
19. Nagaraju, G. V. V. and Rao, G. R., Three phase PUC5 inverter fed induction motor for renewable energy application, International Journal of Power Electronics and Drive System (IJPEDS), Vol.11, No. 1, 2020, https://doi.org/10.11591/ijpeds.v11.i1.pp1-9.
20. Khan, S. A., Guo, Y., Khan, Md. N., Siwakoti, Y. and Blaabjerg, F., A novel single source three phase seven-level inverter topology for grid-tied photovoltaic application, *Proceedings of the 2020 IEEE 9th International Power Electronics and Motion Control Conference (IPEMC-ECCE Asia)*, Nanjing, China, pp. 372–376, November 29-December 2, 2020, https://doi.org/10.1109/IPEMC-ECCEAsia48364.2020.9367731.
21. Kibria, M. F., Mekhilef, S., Mubin, M., Tey, K. S., Elsanabary, A., A hybrid single-phase transformerless solar photovoltaic grid-connected inverter with reactive power capability and reduced leakage current, IEEE Access, Vol. 13, pp 39235–39247, 2025, https://doi.org/10.1109/ACCESS.2025.3546670.

22. Lamreoua, A., Benslimane, A., Boucnaif, J., Hirech, K., Adaliou, A. and El Ouariachi, M., Current harmonic reduction for grid-connected photovoltaic system (PV) based on improved control of three-phase seven-level PUC inverter, Materiels today: Proceedings, Vol. 72, Part 7, p.p 3536-3543, 2023, https://doi.org/10.1016/j.matpr.2022.08.266.
23. Shankar, J., Mallesham, G. and Surrender, R. S., Optimal Tuning of PI Controller for Automatic Generation Control in Multi-Area Power Systems Using PSO for Enhanced Load Frequency Control, Journal of Electrical Systems, Vol. 20, No. 3, 6983-6998, 2024, https://journal.esrgroups.org/jes/article/view/7233, [Accessed: 12. Feb, 2026].
24. Xue, H. and He, J., Adaptive control strategy of parallel cascaded H-bridge PV-battery hybrid inverters for enhanced power balance capability, IEEE Transactions on Industrial Electronics, Vol. 72, No. 1, pp 504–515, 2025, https://doi.org/10.1109/TIE.2024.3406862.
25. Tiwari, A., Kumar, V., Agarwal, R., Amir, M., Alharbi, M. A. and Muyeen, S. M., Five-level MLI-based grid-connected photovoltaic systems: A review on control methodologies, modulation strategies and recent developments, IEEE Open Journal of Power Electronics, Vol. 6, pp 78–108, 2025, https://doi.org/10.1109/OJPEL.2024.3515288.

Paper submitted: 26.08.2025
Paper revised: 14.01.2026
Paper accepted: 18.01.2026